DOI: 10.1002/asia.200800279

Tetramethyl-*m*-benziporphodimethene and Isomeric α,β-Unsaturated γ-Lactam Embedded N-Confused Tetramethyl-*m*-benziporphodimethenes

Gao-Fong Chang,[a] Anil Kumar,[a] Wei-Min Ching,[b] Han-Wei Chu,[a] and Chen-Hsiung Hung*[a]

Abstract: The condensation reaction of α,α′-dihydroxy-1,3-diisopropylbenzene, pyrrole, and an aldehyde leads to the formation of tetramethyl-*m*-benziporphodimethene and outer α-pyrrolic carbon oxygenated N-confused tetramethyl-*m*-benziporphodimethenes containing a γ-lactam ring in the macrocycle. Two isomers with the carbonyl group of the lactam ring either close to (O-Up) or away from (O-Down) the neighboring sp^3 *meso* carbon were synthesized and characterized. The single crystal X-ray diffraction analysis on the regular and γ-lactam containing tetramethyl-*m*-benziporphodimethenes showed highly distorted macrocycles for all compounds. For O-Up and O-Down isomers, dimeric structures, assembling by intermolecular hydrogen-bonding interactions through lactam rings, were observed in the solid state. Fitting the concentration dependent chemical shifts of the outer NH proton using the non-linear regression method give a maximum association constant of 108.9 M^{-1} for the *meso* 4-methylcarboxyphenyl substituted O-Down isomer. The DFT calculations concluded that the O-Up isomer is energetically more stable, and the keto form is more stable than the enol form.

Keywords: density functional calculations · lactams · macrocycles · N-confused · porphyrinoids

Introduction

Large families of expanded, contracted, and isomeric porphyrins were created by changing the number and sequence of the constituent pyrrole rings and carbon linkages.[1,2] The core modifications involving the introduction of a CH unit in the porphyrins, which belongs to a heterocyclic or carbocyclic moiety in place of one of the nitrogen atoms, have led to the preparation of a series of carbaporphyrinoids that have interesting properties in both aromatic character and ability to bind metal ions.[3–7] The first example are N-confused or inverted porphyrins,[4,5,8] which are porphyrin isomers having one of the pyrrolic nitrogens placed on the periphery of the macrocycle rather than in the core. In another group of carbaporphyrinoids, a C–H bond belongs to the inner carbocyclic unit. Such replacements preserve three of the regular pyrrole moieties, while the CNNN core becomes the representation of the monocarbaporphyrinoid structure.[9,10] These macrocycles bear a functional resemblance to certain polydentate ligands,[11–14] which, by virtue of a favorably oriented carbon donor, afford rare organometallic compounds of transition elements, often stabilizing unusual oxidation states or coordination geometries. The carbocycle affects the degree of π conjugation in the system, and consequently, the macrocyclic aromaticity in some carbaporphyrinoids is attenuated or totally absent.[15] *m*-Benziporphyrin, an exemplary system based on a carbocyclic unit, is a class of porphyrin analogue in which the macrocycle is formally constructed from three pyrrole rings and one benzenoid ring that are connected by *meso* bridges.[6,7,16,17] Although the *m*-benziporphyrin exhibits no macrocyclic aromaticity,[16] other systems,[7] such as *p*-benziporphyrin and oxybenziporphyrin, display ring currents comparable to those of regular porphyrins. Coordination chemistry of benziporphyrins has been studied systematically to reveal that these ligands form organometallic complexes with transition metals,[16,18] acti-

[a] G.-F. Chang, A. Kumar, H.-W. Chu, Prof. Dr. C.-H. Hung
Institute of Chemistry
Academia Sinica
128 Academia Road Sec. 2, Nankang
Taipei 11529 (Taiwan)
Fax: (+886) 2-27831237
E-mail: chhung@chem.sinica.edu.tw

[b] W.-M. Ching
Department of Chemistry
National Taiwan Normal University
No. 88, Sec. 4, Ting-Chow Road
Taipei, 11677 (Taiwan)

Supporting information for this article is available on the WWW under http://dx.doi.org/10.1002/asia.200800279.

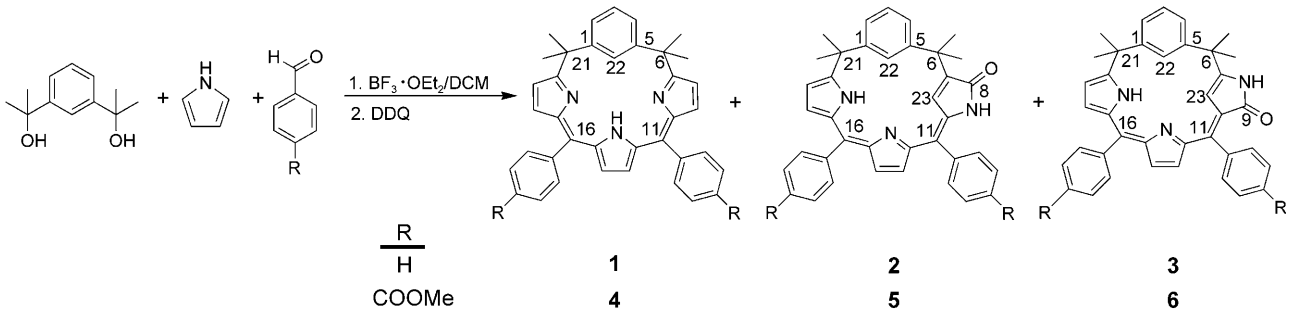

Scheme 1.

vate arene C–H bonds toward oxidative substitutions,[16,19] and stabilize weak metal–arene interactions.[17,20]

The basic structural motif in benziporphyrins may be modified in ways that are similar to the modification of regular porphyrins. The recently synthesized *m*-benziporphodimethene, is a modified *m*-benziporphyrin with two tetrahedral *meso* bridges at positions 6 and 21 (see Scheme 1).[20] In addition to having a similar frame structure as *m*-benziporphyrin, this new type of compound also has the potential to activate the arene C–H bond by insertion of a transition metal. However, knowledge of the chemistry, geometry, and application of this new type of compound is scarce in the literature.[21,22] From the survey of the literature, a confusion approach has been performed extensively with N/O/S-confused porphyrins but not with a benziporphodimethene. In this paper we report on successfully synthesizing two isomeric tetramethyl-*m*-benziporphodimethenes containing a γ-lactam ring which results in a new inner CCNN macrocycle frame. The synthesis, isolation, and single crystal X-ray structures of the newly synthesized isomeric N-confused tetramethyl-*m*-benziporphodimethenes are presented herein. The energetics of these tetramethyl-*m*-benziporphodimethenes was investigated using computational chemistry methods.

Abstract in Chinese:

本篇文獻報導新的苯紫質衍生物的合成及光譜性質：由 α,α′-dihydroxy-1,3-diisopropylbenzene、吡咯和苯甲醛所進行的縮合反應，得到了主產物 tetramethyl-*m*-benziporphodimethene 以及外翻吡咯碳上氧化形成內醯胺環的兩種苯紫質異構物(O-Up 與 O-Down)。晶體結構顯示，此些類紫質環呈現扭曲的結構；亦顯示 O-Up 和 O-Down 兩種化合物，可利用內醯胺環構成分子間氫鍵，形成二聚體。利用改變濃度影響外翻氮上的氫原子的核磁共振位移，計算得到化合物 **4** 有最大的二聚合常數 108.9。此外，密度泛函理論計算結果也顯示，O-Up 型態的大環比 O-Down 型態在能量上較穩定。而內醯胺環的互變異構物中，以酮類的型態存在比烯醇型態穩定。

Results and Discussion

Synthesis and Spectroscopy

Following the literature method for the preparation of *m*-benziporphyrin,[16] the condensation reaction of α,α′-dihydroxy-1,3-diisopropylbenzene, pyrrole, and benzaldehyde using BF_3·OEt_2 as acid catalyst followed by a 2,3-dichloro-5,6-dicyano-*p*-benzoquinone (DDQ) oxidation, as shown in Scheme 1, gave the initially planned 11,16-*bis*(phenyl)-6,6,21,21-tetramethyl-*m*-benziporphodimethene, **1**, after column chromatography. The silica gel column chromatography, however, not only afforded desired **1** (12.6% yield) but also yielded two new types of γ-lactam containing N-confused benziporphodimethenes, O-Up (**2**) in 1.5% yield and a trace amount of O-Down (**3**). Mass spectra showed that these two new compounds have 16 unit mass greater than the parent compound **1**. Efforts were made to increase the yield of compounds **2** and **3** by changing the concentration of acid catalyst and the amount of DDQ. According to the molecular formula, the oxidation from the cyclized porphyrinogen-like unconjugated precursor to **1** requires 2 equiv of DDQ. It was found that the yields of **1**, **2**, and **3** dropped significantly when an insufficient amount of DDQ was used. Using 0.2 equiv of BF_3·OEt_2 and 1.1 equiv of DDQ for the reaction yielded only a trace amount of **2** and **3**. When 3.3 equiv of DDQ was used, a decreased amount of BF_3·OEt_2 resulted in higher yields of **2** and **3**. An optimized reaction condition using 0.2 equiv of BF_3·OEt_2 as acid catalyst and 3.3 equiv of DDQ as oxidant on a 1:3:2 mole ratio of the diol, pyrrole, and benzaldehyde gave yields of 27%, 4%, and 0.7% for **1**, **2**, and **3**, respectively. Alternatively, compound **3** can be synthesized in 8.7% yield using **1** as the starting material through a photochemical reaction (see Experimental Section). When TFA was used as the acid catalyst, the most intense peak on the ESI-mass spectrum of the crude product matched the *m*/*z* value of tetraphenylporphyrin and the mass peak for **1**, which was the most intense peak when BF_3·OEt_2 was used as catalyst, was completely absent. The synthesis of compounds with an ester group substituted on the *meso* phenyl ring using methyl 4-formylbenzoate as the starting aldehyde, yielded compounds **5** and **6** in yields of 2.9% and 1.3%, respectively, along with **4** in 11% yield. The 4-methylcarboxyphenyl substituted derivatives obey the

same absorption spectra profile and NMR spectra pattern as the phenyl substituted compounds.

Though several reports described peripheral oxygenation on porphyrinic macrocycles during the synthesis of a desired compound or upon DDQ oxidation,[8,23,24] it is rare to collect all structural isomers in a one-pot reaction. In our case, oxygenated N-confused tetramethyl-*m*-benziporphodimethenes, both O-Up and O-Down, were isolated during the synthesis of **1** and **4**. Intriguingly, synthesis of **3** from **1** through a photochemical reaction involves bond breaking and bond formation and results in an N-confused CCNN inner core from an originally CNNN inner core structure. To our knowledge, this is the first example of a CCNN core *m*-benziporphodimethene having oxygenation at the inverted pyrrole ring of the macrocycle.

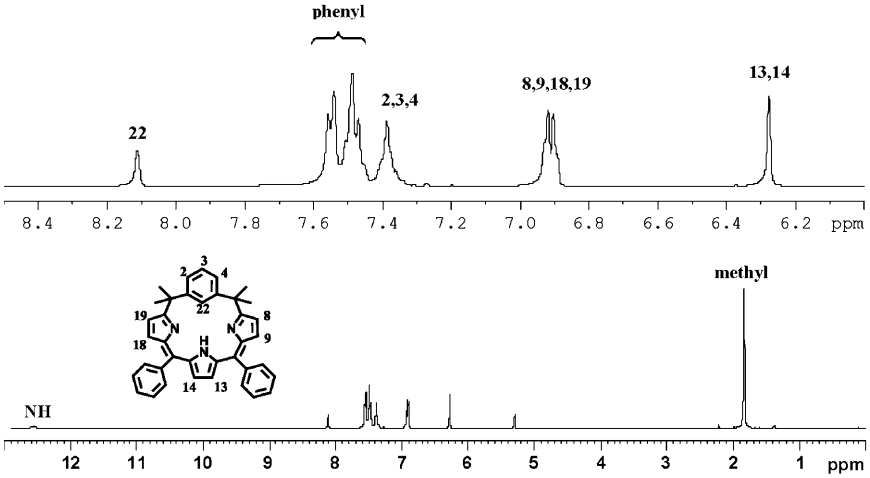

Figure 1. ^{1}H NMR spectra of **1** in $CDCl_3$ at 298 K. The upper diagram shows the expanded region and the structure of **1**.

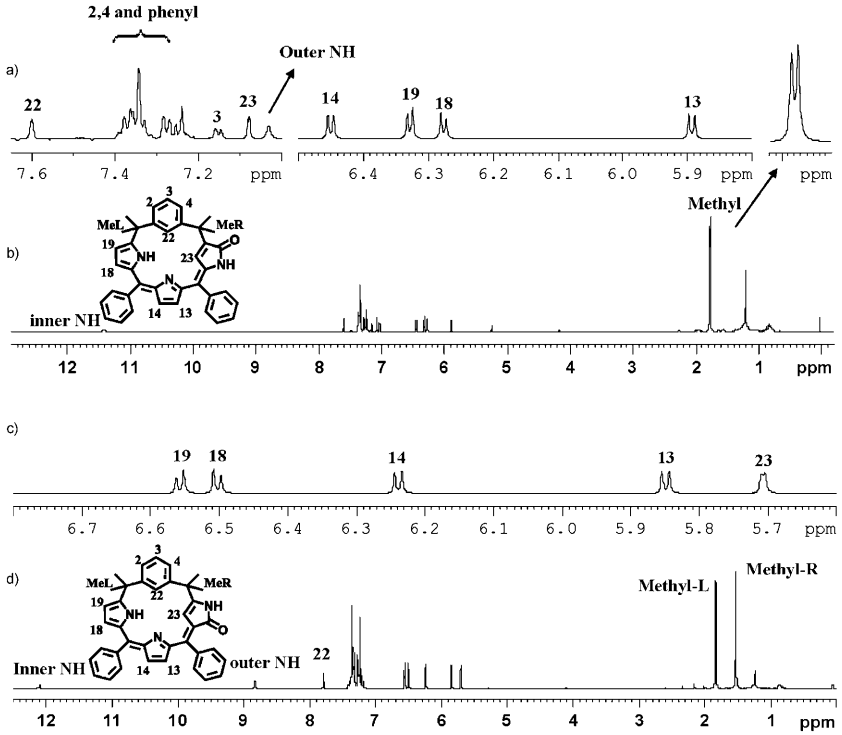

Figure 2. ^{1}H NMR spectra of **2** and **3** recorded in $CDCl_3$ at 298 K: (a) ^{1}H NMR spectra of **2** in selected region; (b) Full range ^{1}H NMR spectra of **2**; (c) ^{1}H NMR spectra of **3** in selected region; (d) Full range ^{1}H NMR spectra of **3**.

^{1}H NMR of tetramethyl-*m*-benziporphodimethene, **1**, in $CDCl_3$ showed a symmetrical pattern with a singlet at 1.75 ppm integrated into twelve hydrogens corresponding to four methyl groups on two sp^3-hybridized *meso* carbons. The signal for hydrogen on C(22) appeared at 8.00 ppm and the resonance for an NH proton inside the core was located at 12.46 ppm as a broad resonance (Figure 1). As shown in Figure 2, the ^{1}H NMR spectra of compounds **2** and **3** are much more complicated. In the case of **2**, because oxygenation on the inverted pyrrole ring breaks the plane of symmetry, the resonances of the twelve hydrogens on the methyl groups split into two peaks at 1.77 and 1.78 ppm. The characteristic doublet ($^4J_{HH}$ = 1.65 Hz) signal at 7.08 ppm corresponds to the hydrogen on C(23) (internal carbon) and resonance for the hydrogen on C(22) appears as a singlet at 7.60 ppm. The amino protons inside and outside the core for **2** are observed as singlets at 11.42 and 7.03 ppm, respectively. In the case of **3**, the twelve methyl hydrogens also separate into two groups with resonances at 1.53 and 1.83 ppm. The hydrogen on C(23) of **3** appears at 5.71 ppm as a doublet ($^4J_{HH}$ = 2.12 Hz) which is shifted upfield by 1.37 ppm in comparison with the value observed from **2**. The difference in the chemical shift for the proton on C(23) of **2** and **3** is likely to arise as a result of a different degree of inductive effect. While an electron-withdrawing carbonyl group locates in the terminal of a conjugation system in **2** and directly downfield shifts the proton signal of C(23), there is no conjugation system connecting the car-

bonyl group and the inner pyrrolic double bond on C(23) in **3**. Noticeably, the 8.84 ppm for the outer NH proton in **3** is shifted downfield by 1.81 ppm compared to the value of 7.03 in **2**. The assignments of resonances for **2** and **3** were confirmed by peak correlations on NOESY and HSQC spectra (see the Supporting Information). In the ^{1}H NMR spectra of **4**, **5**, and **6**, which can be found in the Supporting Information, all the protons on the periphery of the macrocycle show resonances that are nearly identical with the corresponding resonances for compounds **1**, **2**, and **3**, respectively. For compound **4**, the resonance of hydrogens on the ester group appears at 3.94 ppm as a singlet and the singlet at 1.73 ppm is from the twelve hydrogens on the *meso* methyl groups. Because of the different chemical environments, the protons on the two ester groups for **5** and **6** exhibit different resonances, that is, 3.929 and 3.932 ppm for **5** and 3.888 and 3.925 ppm for **6**. As is observed from the ^{1}H NMR spectra of **2** and **3**, in compounds **5** and **6**, the peaks for the protons on the methyl groups separate into two different chemical shifts, each integrated into six hydrogens, at 1.77 and 1.81 ppm for **5** and at 1.48 and 1.84 ppm for **6**.

The absorption spectra for compounds **1**, **2**, and **3** show different profiles with a higher energy Soret-like band at 351 and 350 nm for **1** and **2**, respectively. Split absorptions at 329 and 395 nm are observed for compound **3**. Broad bands in the visible region are observed with absorption maxima at 518, 550, and 709 nm for **1**, 550 nm for **2**, and 560 nm for compound **3** in dichloromethane (Figure 3). The profiles for the absorption spectra appear to be independent

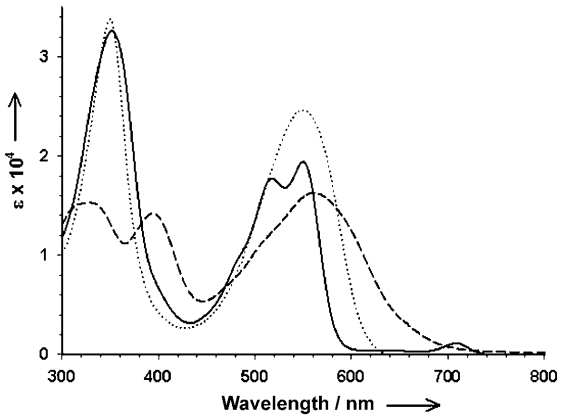

Figure 3. Absorption spectra of **1** (solid line), **2** (dotted line), and **3** (dash line) in dichloromethane.

of the *meso* substitutents. Split Soret-like bands at 314 and 353 nm for **4** are observed. A sharp high energy band at 352 nm for **5** and split bands at 312 and 398 nm are observed for **6**. Broad bands in the low energy visible region are observed with absorption maximum at 518 and 550 nm for **4**, 554 nm for **5**, and 570 nm for **6** in dichloromethane.

Single Crystal X-ray Structures

The explicit structures of **1**, **2**, and **3** are elucidated by single crystal X-ray diffraction analyses (Figure 4). For **2** and **3**, the assignment of the inner-carbon atom and outer-nitrogen

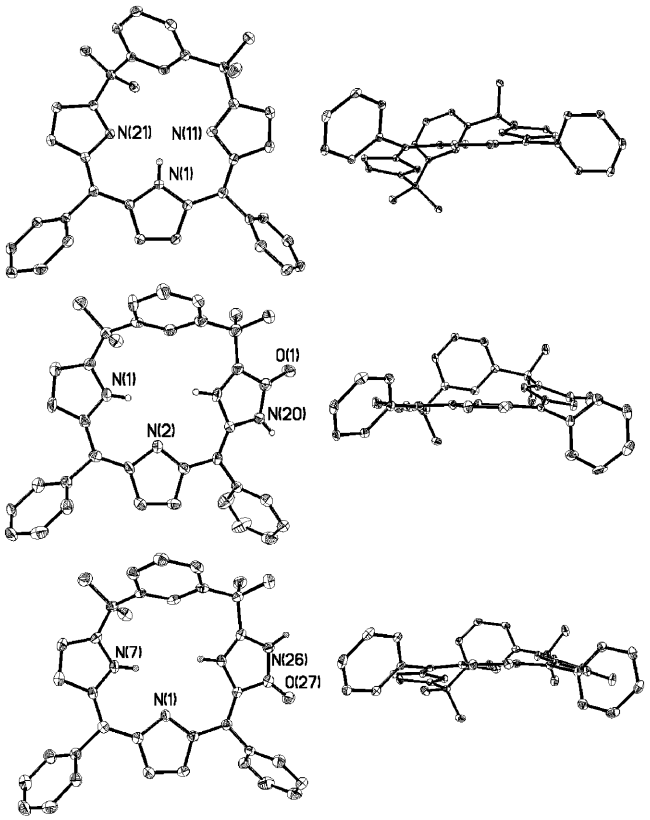

Figure 4. Top view (left column) and side view (right column) on the X-ray structures of **1**, **2**, and **3** (from top to bottom).

atom, which constitute the inverted pyrrole ring, was conducted based on the thermo-parameters. A convergence on the refinement could not be reached if, instead, an inner nitrogen and an outer carbon were assigned on the oxygenated five-membered ring. In all cases, the positions of the hydrogens can be located directly from the electron density map. The difference between the isomeric **2** and **3** is on the locations of the oxygen and nitrogen atoms on the inverted pyrrole ring. In the structural isomers of **2** and **3**, compound **2** has the oxygen of the γ-lactam moiety in close vicinity to the macrocyclic phenylene ring and in the structure of **3**, it is found below the phenylene ring. Analysis of the single crystal X-ray structures reveal that the ring conformation of the macrocycle in **1** is much more distorted than **2** and **3**. The average deviation of 25 atoms on the macrocycle from a mean tripyrrin plane for **1** is 1.044 Å while the values for **2** and **3** are 0.680 and 0.630 Å, respectively. The angle between the CN_2 inner-core plane and the macrocyclic–phenylene plane is 70.35° for **2** and 69.76° for **3**, but in case of **1**, the angle between the phenylene plane and the three pyrrolic

nitrogen plane is only 52.39°. Another interesting feature in the crystal structure is that the angle between the vector along two sp^3 *meso* carbons and the plane, defined by the mean plane of 17 atoms on a tripyrrin moiety, is 28.51° for **1**, which is significantly larger than 15.79° and 14.34° for **2** and **3**, respectively. These data are in good agreement with the fact that **2** and **3** are less puckered than **1** with the phenylene rings oriented vertical to the mean plane of the macrocycles.

On the lactam rings, the C=O bond distance of O-Up and O-Down differs slightly, that is, 1.221(3) and 1.236(2) Å for **2** and **3**, respectively. Nevertheless, both values are within the double bond range suggesting that the keto form dominates in the solid-state structures. In the crystal lattice of **2** and **3** (Figure 5), intermolecular hydrogen-bonding interactions through γ-lactam moieties on two neighboring molecules were observed, with an amino group as hydrogen-bonding donor and a carbonyl group as hydrogen-bonding acceptor, to form dimeric structures. Consistent with a longer C=O bond length in **3**, the distance of 2.777 Å in **3** from hydrogen bonded oxygen to nitrogen is shorter than 2.789 Å in **2** and suggests stronger intermolecular hydrogen-bonding interactions for **3**. Analysis of space-filled models on pairs of hydrogen-bonded molecules revealed a larger steric constraint from the methyl group to the nearby *meso* phenyl ring for **2**, which contributes to the weakening of the hydrogen-bonding interactions. The effect of steric constraint as a result of intermolecular interactions also reflects on the conformation of the macrocycles. As shown in Figure 4, because of the steric constraint, the solid state structure of **2** adopted a more distorted geometry with a larger deviation of the phenylene ring from the tripyrrin unit in comparison with a near co-planar conformation in **3**.

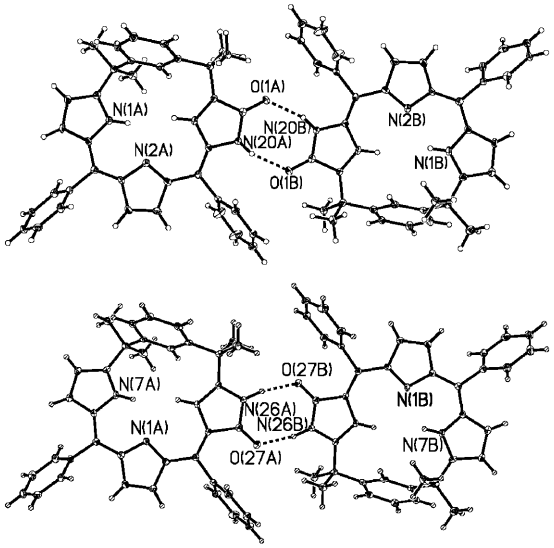

Figure 5. Intermolecular hydrogen-bonding interactions between **2** (upper diagram) and **3** (lower diagram) through lactam moiety. The hydrogen-bonding distance is 1.941 Å for **2** and 1.825 Å for **3**.

Formation of Self-Association Dimers Evaluated by Association Constants

As described above, the solid state crystal structures of **2** and **3** assemble as dimers through hydrogen bonding of the lactam amide bond. To reveal the potential interactions in solution, association constants were obtained from the concentration dependent chemical shifts of **2**, **3**, **5**, and **6** in $CDCl_3$. In the ^1H NMR spectra of compound **2**, the outer NH proton′s resonance is shifted downfield by 0.115 ppm when the concentration increases from 1.00×10^{-3} to 5.25×10^{-2} M while in **3**, under the same conditions, the downfield shift for the NH proton is as large as 1.949 ppm. The larger chemical shift change implies a higher degree of dimerization in the solution of **3**. In addition, as shown in Table 1, most of the proton resonances in **2**, **3**, **5**, and **6** display a trend of either a downfield or an upfield shift when the concentration is increased. As expected, the *meso* methyl groups in the vicinity of the lactam ring, MeR, have the second largest chemical shift difference after the outer NH proton. The MeR shifted downfield by 0.013 ppm when the concentration of **2** was increased from 1.00×10^{-3} to 5.25×10^{-2} M, but, intriguingly, an upfield shift of 0.087 ppm for MeR was observed in **3** when the concentration was in-

Table 1. Concentration dependent ^1H NMR chemical shifts for the protons on **2**, **3**, **5**, and **6**.

	Conc. [$\times10^{-2}$ M]	outer NH	H13	H14	H18	H19	H23	H22	MeL	MeR
2	0.10	6.9664	5.9192	6.4758	6.3023	6.3551	7.1066	7.6287	1.8103	1.8028
	5.25	7.0818	5.9271	6.4826	6.3088	6.3612	7.1159	7.6358	1.8168	1.8159
	Δ	+0.1154	+0.0079	+0.0068	+0.0065	+0.0061	+0.0093	+0.0071	+0.0065	+0.0131
3	0.1	7.3500	5.8282	6.2423	6.5008	6.5510	5.7548	7.7905	1.8543	1.6019
	5.00	9.2988	5.8604	6.2426	6.5069	6.5626	5.6990	7.8002	1.8406	1.5146
	Δ	+1.9488	+0.0322	valley	+0.0061	+0.0116	−0.0558	+0.0097	−0.0137	−0.0873
5	0.1	6.9347	5.8713	6.4231	6.2470	6.3650	7.1026	7.6068	1.8107	1.7990
	4.20	7.4423	5.8705	6.4194	6.2441	6.3626	7.0932	7.5991	1.8078	1.7576
	Δ	+0.5076	−0.0008	−0.0037	−0.0029	−0.0024	−0.0094	−0.0077	−0.0029	−0.0424
6	0.1	7.4795	5.7734	6.1879	6.4322	6.5591	5.7485	7.7721	1.8350	1.5926
	5.07	9.7077	5.8221	6.1885	6.4404	6.5724	5.6722	7.7698	1.8376	1.4607
	Δ	+2.2282	+0.1087	valley	+0.0082	+0.0133	+0.0763	valley	+0.0026	−0.1319

Δ: The difference of chemical shifts at low and high concentration. The values are positive for a downfield shift and are negative for an upfield shift when the concentration of the solution was increased; valley denotes that no clear trend was observed.

creased. The opposite direction of the changes in the chemical shift for MeR in **2** and **3** is likely a result of different spatial orientation which generates different types of ring-current effects between the *meso* phenyl ring and the nearby MeR. While the O-Up isomer, **2**, gives a closed-contact with MeR directing toward the periphery of the phenyl ring, while the MeR orients toward the center of the ring current in **3**.

Careful examination of the chemical shift change reveals downfield shifts of 0.508 and 2.228 ppm for the outer NH proton in **5** and **6**, respectively, when the concentration increases from 1.00×10^{-3} to 4.20×10^{-2} M for **5** and from 1.00×10^{-3} to 5.07×10^{-2} M for **6**. The chemical shift changes are larger in **5** and **6** than the corresponding values of 0.013 and 1.949 ppm in **2** and **3**, respectively. Concerning the chemical shift of MeR, the values shifted upfield by 0.042 and 0.132 ppm for **5** and **6**, respectively, when the concentration was increased. The larger chemical-shift difference of MeR in **5** and **6** also supports the higher tendency of dimerization with 4-methylcarboxyphenyl substituents. According to the chemical shifts, it appears that compound **6** has the largest dimerization equilibrium constant. In addition to intermolecular hydrogen-bonding interactions between amide bonds, additional effects from, for example, hydrogen-bonding interactions between the carbonyl group of methylcarboxyphenyl and MeR or between methylcarboxyphenyl C=O and the inner NH protons might also contribute to a higher degree of self-aggregation.

$$\delta_{obs} = \delta_m + (\delta_d - \delta_m)\frac{\sqrt{1+8K_a[A]_0}-1}{\sqrt{1+8K_a[A]_0}+1} \quad (1)$$

The use of Equation (1) for non-linear regression curve fittings on the plots of chemical shifts (δ_{obs}) vs concentration ([A]) based on the resonances of the outer NH proton gives the desired association constants (K_a).[25] As shown in Figure 6, the association constant of 72.3 M^{-1} for **3** is more than two orders of magnitude higher than the value of 0.57 M^{-1} for **2**. This result obtained from ^{1}H NMR in solution is consistent with a longer carbonyl C=O bond distance and a shorter hydrogen-bonding distance for **3** in the solid state crystal structure in comparison with **2**. According to the plot, the chemical shifts of the outer NH proton on the lactam ring in the monomeric (δ_m) and dimeric (δ_d) state are calculated to be 6.96 and 9.14 ppm for **2** and 6.94 and 10.26 ppm for **3**. For **5** and **6**, the association constants of 12.3 and 109.8 M^{-1}, respectively, are obtained and the chemical shifts for the monomeric and dimeric state of the outer NH proton are 6.89 and 8.35 ppm for **5**, and 6.88 and 10.68 ppm for **6**. In comparison with other self-association systems, the values of **3** and **6** are comparable with other lactam ring containing macrocycles in the literature and are much larger than the value of 0.166 M^{-1} obtained from the dimerization of 2-aminopyridine.[25–27]

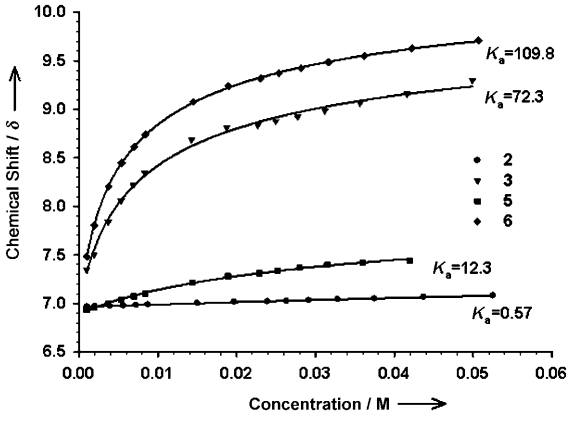

Figure 6. Plot of the observed chemical shift of the outer NH group vs concentration for **2**, **3**, **5**, and **6**. The association constants were obtained by curve fitting to Equation (1).

To evaluate the potential of using the lactam ring containing benziporphodimethene as an effective compound for molecular recognition,[8,23a] both **5** and **6**, at a concentration of 6.2×10^{-3} M to act as hosts, were treated with an increasing amount of the guest molecule, 2-aminopyrimidine. A 0.38 ppm shift downfield for the resonance of the outer NH proton was observed when 10 equiv of 2-aminopyrimidine was added to the $CDCl_3$ solution of **5**, while, under the same conditions, a 0.17 ppm downfield shift was observed for **6**. Interestingly, when applied to this host–guest recognition system, compound **5** appears to have a higher association constant in comparison with **6**, probably because more monomeric compound **5** is available for interacting with guest molecules. Because of the complicated intermolecular interactions of forming 1:1 and 2:1 host–guest complexes as well as the presence of self-association dimers for host and guest molecules, no effort was attempted to obtain the equilibrium constant in the host–guest systems.

Density Functional Calculation

Density functional theory methods have been successfully used to calculate the electronic structures of porphyrins and their related analogues to provide information on their energetics, conformational behavior, tautomerism, and aromaticity.[28] In this work we have isolated new isomeric N-confused *m*-benziporphodimethenes containing a γ- lactam ring, **2** and **3** during the synthesis of **1**. From the conjugation system point of view, **2** has a longer conjugation length than **3** and involves 14π electrons in one delocalization path in comparison with the longest 12π electron delocalization path in **3**. Similar pathways of conjugation in **2** and **3** have been observed in **5** and **6**, respectively. We are curious to know, of the two isomeric confused benziporphodimethenes, which structure is energetically more favorable. Also, it is desirable to know the energy difference between regular tetramethyl-*m*-benziporphodimethene and its inverted isomers as well as enthalpy changes during the formation of hydrogen bonded dimers. To address these issues, we have carried out full geometry optimization DFT[29] calculations on compounds **1**, **2**, and **3** using the B3LYP/6-311+G(d,p)//B3LYP/6-31G(d,p) level of theory. DFT studies were also carried

out on inverted isomers of tetramethyl-*m*-benziporphodimethenes, **1-1** and **1-2**, using the same level of theory in the gas phase. Initial geometries were taken from the single crystal X-ray structure determinations. The structures on isomers of *m*-benziporphodimethene and oxygenated N-confused *m*-benziporphodimethene are given in Scheme 2. The relative

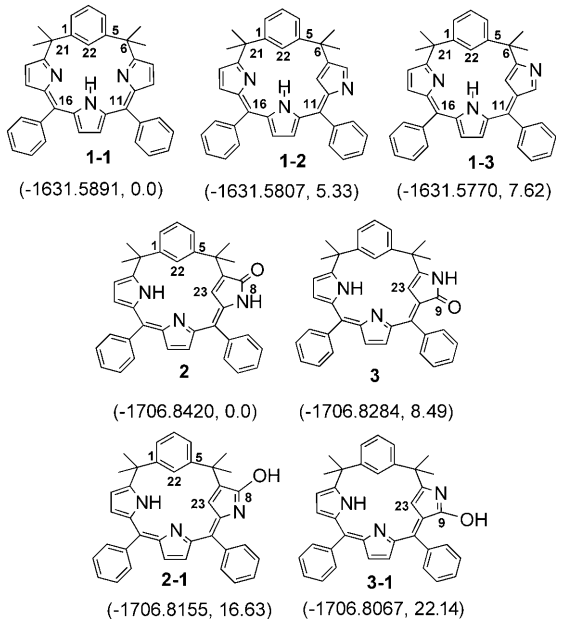

Scheme 2. Different isomers of *m*-benziporphodimethes on which DFT calculations were carried out. The total energies (in Hartree) and relative energies (in kcal mol^{-1}) with respect to **1** for pyrrole based macrocycles and to **2** for lactam based macrocycles are given in parentheses.

energies for each series of molecules are given in parenthesis below the molecule code and also summarized in Table S1 of the Supporting Information. Since **2** and **3** contain a γ-lactam moiety, the existence of keto–enol tautomerism through intramolecular hydrogen bonding is of interest. Therefore, we have also carried out DFT calculations on their enol forms **2-1** and **3-1** and compared the relative energies with the keto tautomers **2** and **3**.

As shown in Scheme 2, the energy differences between **1** and its inverted isomers **1-1** and **1-2** are 5.33 and 7.62 kcal mol^{-1}, respectively. The inner core hydrogen-bonding interaction between NH and the imino nitrogen apparently plays an important role in stabilizing the isomer **1** in comparison to **1-1** and **1-2** as in the case of tetraphenylporphyrin vs N-confused tetraphenylporphyrin.[30] The inner NH group can have a hydrogen-bonding interaction with two inner-core imino nitrogens in **1** but, in **1-1** and **1-2**, only one imino nitrogen is available to have such an interaction. Furthermore, in comparison with **1-2**, the position of the peripheral α-pyrrolic CH close to the sp^3 carbon, as in the case of **1-1**, releases the steric interaction between the α-pyrrolic CH and *ortho* protons of the nearby *meso* phenyl ring to stabilize the structure of **1-1**. Among the two isomeric N-confused benziporphodimethenes, it is evident that structure **2** O-Up is energetically more stable than **3** O-Down by 8.49 kcal mol^{-1}. The reason may arise from the longer conjugation in **2**, which stabilizes the structure of **2**. Same orders for total energy were observed in the series of compounds with 4-methylcarboxyphenyl substituents on the *meso* positions. (see Scheme S1 in the Supporting Information) Importantly, the DFT[27] calculations on the enol forms, **2-1** and **3-1**, showed increases of 16.63 kcal mol^{-1} and 13.65 kcal mol^{-1} comparing with their corresponding keto tautomer of **2** (O-Up) and **3** (O-Down), respectively, and increases of 16.23 and 14.00 kcal mol^{-1} were calculated for the enol forms with 4-methylcarboxyphenyl substituted, in comparison with the corresponding keto isomers. The HOMO–LUMO energy gaps among the structure **1**, **2**, and **3** are 2.6, 2.5, and 2.3 eV, respectively, and similar energy gaps are obtained for their 4-methylcarboxyphenyl substituted compounds, which indicates that ester substituents will not affect the electronic structure of macrocycles. The strength of dimeric association assembling through hydrogen-bonding interactions for **2** (O-Up) and **3** (O-Down) was evaluated through the difference between the total energy of two independent molecules and a dimeric molecule optimized from crystal structures. Although the gas phase was assumed for the DFT calculation, the larger decrease in enthalpy with a value of 20.43 kcal mol^{-1} for the dimerization of the O-Down isomer **3** in comparison with the value of 12.13 kcal mol^{-1} for **2** is in good agreement with a stronger intermolecular hydrogen-bonding interaction in **3** than in **2**.[31]

Conclusions

In the present work we have reported on the synthesis of tetramethyl-*m*-benziporphodimethene and its N-confused analogues with an oxygenation on the inverted pyrrole ring leading to a CCNN frame. For the first time, both isomers of γ-lactam containing N-confused tetramethyl-*m*-benziporphodimethenes are isolated and structurally characterized. The crystal structures of γ-lactam containing N-confused tetramethyl-*m*-benziporphodimethenes form dimeric structures through intermolecular hydrogen-bonding interactions. The association constant study suggests that the O-Down isomer with the carbonyl away from the neighboring sp^3 carbon exhibits a stronger intermolecular hydrogen-bonding interaction. Computational chemistry suggests that the keto form of oxygenated N-confused tetramethyl-*m*-benziporphodimethenes, as isolated, are more stable than their enol forms. DFT calculations also demonstrate that regular tetramethyl-*m*-benziporphodimethenes are more stable than their inverted isomers. The new type of macrocyclic frame with a CCNN core is being explored in our lab to study the coordination chemistry of these isomeric species. Also, considering that the amido unit is prevalent in biological molecules, it will be intriguing to adopt the hydrogen-bonding capability in lactam containing N-confused benziporphodimethene for the design of other molecular recognition systems with biological significance.

Experimental Section

Reagents

Pyrrole (Merck) and benzaldehyde (Riedel-de Haën) were redistilled prior to use whereas α,α′-dihydroxy-1,3-diisopropylbenzene (TCI) and boron trifluoride ethyl ether complex (TCI), 2,3-dichloro-5,6-dicyano-*p*-benzoquinone (DDQ, Acros) were used as supplied. All other reagents and solvents were of high purity and were used as purchased without any further purification. $CDCl_3$ (Aldrich) was distilled over CaH_2 and stored in an inert atmosphere glove box. Basic alumina oxide (0.063~0.2 mm) and silica gel (0.04~0.063 mm) were obtained from Merck.

General Procedure

Electronic spectra were recorded at 298 K with an Agilent 8453 spectrophotometer. IR measurements were carried out with a Perkin–Elmer Paragon 1000 spectrophotometer. NMR spectra were recorded on a Bruker Spectrospin 400 Ultra Shield spectrometer. NMR spectra were referenced to residual solvent signals. X-ray single-crystal structures were determined using a Bruker Apex X8 single crystal diffractometer equipped with a 4 K Apex II CCD detector. High resolution mass data was obtained using a JEOL JMS-700 mass spectrometer. Elemental analyses were carried out on a Perkin–Elmer 2400CHN elemental analyzer. Photoirradiations were carried out in a Penchum Photochemical PR-2000 photo-reactor fitted with sixteen 8W G8T5E UVB lamps (Sankyo, Denki, Japan) with a maximum intensity at 302 nm. Column chromatography was routinely carried out using the gravity-feed-column technique on Merck silica gel. Analytical thin-layer chromatography (TLC) analyses were performed on Merck silica gel 60 F_{254} precoated aluminum sheets.

*Synthesis of **1**, **2**, and **3***

A solution of α,α′-dihydroxy-1,3-diisopropylbenzene (98 mg, 0.50 mmol), benzaldehyde (102 μL, 1.01 mmol), and pyrrole (104 μL, 1.51 mmol) in CH_2Cl_2 (150 mL) was treated with $BF_3{\cdot}OEt_2$ (13 μL, 0.10 mmol) and stirred at 27 °C. Two hours later, DDQ (374 mg, 1.65 mmol) was added into the reaction mixture, and continuously stirred for 2 h at 27 °C. The reaction was quenched with triethylamine and the solvent was removed in vacuo. The crude mixture was dissolved in a minimum amount of CH_2Cl_2 and was purified using silica gel column chromatography (400 mL) eluting with CH_2Cl_2 to give **1** (72 mg, 27%) as a red powder, **2** (11 mg, 4%) as a red powder, and **3** (2 mg, 0.8%) as a purple powder. Alternatively, **3** can be synthesized from **1** with a higher yield through a photochemical reaction. The details of this reaction are provided later.

1: R_f=0.11 (CH_2Cl_2); UV/Vis (CH_2Cl_2): $\lambda(\varepsilon)$=550 (19500), 518 (17400), 349 nm (32300); ^{1}H NMR (400 MHz, $CDCl_3$, 25 °C): δ=12.46 (br, 1H, NH), 8.00 (s, 1H, 22-ArH), 7.29–7.48 (m, 13H, 2,3,4-ArH and *meso*-ArH), 6.83 (*ab* quartet, $^3J_{H,H}$=4.54 Hz, 4H, 8,9,18,19-PyrrH), 6.19 (s, 2H, 13,14-PyrrH), 1.75 ppm (s, 12H, CH_3); ^{13}C NMR (400 MHz, $CDCl_3$, 25 °C): δ=182.20, 152.15, 147.38, 139.05, 138.46, 138.27, 136.83, 131.94, 129.06, 128.54, 127.78, 127.45, 125.12, 123.32, 121.50, 42.33, 29.17 ppm; HRMS (FAB): *m*/*z* (%) calcd for $C_{38}H_{34}N_3$: 532.2752 $[M+H]^+$; found: 532.2745 (100); elemental analysis: calcd (%) for $C_{38}H_{33}N_3{\cdot}0.5\,C_6H_{14}$: C 85.67, H 7.01, N 7.31; found: C 84.08, H 7.32, N 7.31.

2: R_f=0.59 (CH_2Cl_2); UV/Vis (CH_2Cl_2): $\lambda(\varepsilon)$=550 (24500), 350 nm (33900); ^{1}H NMR (400 MHz, $CDCl_3$, 25 °C): δ=11.42 (br, 1H, NH), 7.60 (s, 1H, 22-ArH), 7.23–7.37 (m, 12H, 2,4-ArH and *meso*-ArH), 7.15 (m, 1H, 3-ArH), 7.08 (d, $^4J_{H,H}$=1.65, 23-PyrrH), 7.03 (s, 1H, NH), 6.45 (d, $^3J_{H,H}$=4.44, 1H, 14-PyrrH), 6.33 (d, $^3J_{H,H}$=4.00, 1H, 19-PyrrH), 6.28 (d, $^3J_{H,H}$=4.05, 1H, 18-PyrrH), 5.89 (d, $^3J_{H,H}$=4.45, 1H, 13-PyrrH), 1.78 (s, 6H, CH_3), 1.77 ppm (s, 6H, CH_3); ^{13}C NMR (400 MHz, $CDCl_3$, 25 °C): δ=169.88, 157.31, 148.23, 147.20, 146.95, 146.60, 137.56, 135.72, 135.64, 133.42, 132.03, 130.71, 130.13, 128.82, 128.77, 128.52, 128.50, 127.40, 125.61, 125.24, 124.17, 122.67, 120.13, 109.26, 40.90, 40.88, 39.45, 39.43, 28.14, 26.84 ppm; HRMS (FAB): *m*/*z* (%) calcd for $C_{38}H_{34}N_3O$: 548.2702 $[M+H]^+$; found: 548.2708 (100); elemental analysis: calcd (%) for $C_{38}H_{33}N_3O{\cdot}0.3CH_2Cl_2$: C 80.25, H 5.91, N 7.33; found: C 80.72, H 6.07, N 5.99.

3: R_f=0.26 (CH_2Cl_2); UV/Vis (CH_2Cl_2): $\lambda(\varepsilon)$=561 (15800), 395 (14100), 329 nm (15100); ^{1}H NMR (400 MHz, $CDCl_3$, 25 °C): δ=12.10 (br, 1H, NH), 8.84 (s, 1H, NH), 7.79 (s, 1H, 22-ArH), 7.15–7.38 (m, 13H, 2,3,4-ArH and *meso*-ArH), 6.56 (d, $^3J_{H,H}$=4.36, 1H, 19-PyrrH), 6.50 (d, $^3J_{H,H}$=4.24, 18-PyrrH), 6.24 (d, $^3J_{H,H}$=4.28, 1H, 14-PyrrH), 5.82 (d, $^3J_{H,H}$=4.28, 1H, 13-PyrrH), 5.71 (d, $^4J_{H,H}$=2.12, 1H, 23-PyrrH), 1.83 (s, 6H, CH_3), 1.53 ppm (s, 6H, CH_3); ^{13}C NMR (400 MHz, $CDCl_3$, 25 °C): δ=170.73, 170.53, 153.91, 152.68, 148.61, 144.94, 143.04, 139.67, 138.95, 137.41, 131.49, 130.80, 129.89, 128.69, 128.65, 127.98, 127.95, 127.57, 127.30, 127.22, 126.18, 125.93, 123.57, 123.04, 116.32, 102.07, 53,50, 40.64, 28.05, 27.60 ppm; HRMS (FAB): *m*/*z* (%) calcd for $C_{38}H_{34}N_3O$: 548.2702 $[M+H]^+$; found: 548.2706 (100); elemental analysis: calcd (%) for $C_{38}H_{34}N_3O$: C 83.32, H 6.08, N 7.68; found: C 82.64, H 6.02, N 7.40.

*Synthesis of **3** through Photochemical Reactions*

In a quartz tube, **1** (28 mg, 0.05 mmol) was dissolved in CH_2Cl_2 (15 mL) and sealed with a rubber septum. O_2 gas was bubbled into the solution for 5 min. The O_2 saturated solution of **1** was exposed to UV light (302 nm) for 24 h. The solvent was removed in vacuo and the crude solid was dissolved in a minimum amount of CH_2Cl_2 and was purified using silica gel column chromatography using CH_2Cl_2 as an eluent. The first purple band was collected and dried in vacuo to obtain a purple solid of **3**. (2.5 mg, 8.7%) The hexane/dichloromethane/ethyl acetate (7:3:2) mixed solvent was used to recover unreacted **1** as a red solid (21.6 mg, 77%). The UV/Vis spectrum, ^{1}H NMR and mass spectrum of **3**, obtained from the photochemical reaction, were confirmed to be identical to **3** obtained from the acid-catalyzed condensation reaction described previously.

*Synthesis of **4**, **5**, and **6***

A solution of α,α′-dihydroxy-1,3-diisopropylbenzene (194 mg, 1 mmol), methyl 4-formylbenzoate (328.3 mg, 2 mmol) and pyrrole (208 μL, 3 mmol) in CH_2Cl_2 (900 mL) was treated with $BF_3{\cdot}OEt_2$ (100 μL, 0.81 mmol) and stirred at room temperature for 2 h. DDQ (750 mg, 3.3 mmol) was added to the reaction mixture, and continuously stirred for another 30 min at room temperature. The solvent was removed in vacuo. The crude mixture was dissolved in a minimum amount of CH_2Cl_2 and was purified using column chromatography packed with slurry silica gel in CH_2Cl_2. Byproducts from the reaction mixture were eluted out using CH_2Cl_2 and the mixture of **4**, **5**, and **6** was eluted out using a 7:3:2 ratio of hexane, CH_2Cl_2, and ethyl acetate. The collected mixture of solution was evaporated under reduced pressure on a rotovap. The solid residue was further dissolved in CH_2Cl_2, loaded on top of a column packed with silica gel in CH_2Cl_2, and eluted by the same ratio of hexane, CH_2Cl_2, and ethyl acetate. The first red fraction of **4** collected contained impurity and was used for further chromatography, while pure solutions of **5** and **6** were eluted out as second and third major fractions, respectively. Analytical pure compounds of **5** (19 mg, 2.9%) and **6** (8.3 mg, 1.25%) were obtained after solvent removal. The solid of **4** was dissolved in a minimum amount of CH_2Cl_2, loaded to a silica gel column, and eluted using CH_2Cl_2. The impurity was discarded and the pure solution of **4** was eluted out using the mixture of hexane, CH_2Cl_2, and ethyl acetate in a ratio of 7:3:2. The solvent was removed in vacuo to give **4** as a red powder (71.3 mg, 11%).

4: R_f=0.78 (hexane/CH_2Cl_2/ethylacetate=7:3:2); UV/Vis (CH_2Cl_2): $\lambda(\varepsilon)$=550 (21900), 518 (20000), 353 (32400), 314 nm (27500); ^{1}H NMR (400 MHz, $CDCl_3$, 25 °C): δ=12.34 (br, 1H, NH), 8.07 (d, $^3J_{H,H}$=8.28, 4H, *meso-meta*-ArH), 7.94 (s, 1H, 22-ArH), 7.52 (d, $^3J_{H,H}$=8.32, 4H, *meso-ortho*-ArH), 7.24–7.28 (m, 3H, 2,3,4-ArH), 6.83 (d, $^3J_{H,H}$=4.60, 2H, 8,19-pyrrH), 6.75 (d, $^3J_{H,H}$=4.64, 2H, 9,18-PyrrH), 6.08 (s, 2H, 13,14-PyrrH), 3.94 (s, 6H, OCH_3), 1.73 ppm (s, 12H, CH_3); HRMS (ES): *m*/*z* (%) calcd for $C_{42}H_{38}N_3O_4$: 648.2862 $[M+H]^+$; found: 648.2856 (100).

5: R_f=0.48 (hexane/CH_2Cl_2/ethylacetate=7:3:2); UV/Vis (CH_2Cl_2): $\lambda(\varepsilon)$=554 (24000), 352 nm (28800); ^{1}H NMR (400 MHz, $CDCl_3$, 25 °C): δ=11.41 (br, 1H, NH), 8.08 (d, $^3J_{H,H}$=8.28, 2H, *meso-meta*-ArH), 8.04 (d, $^3J_{H,H}$=8.36, 2H, *meso-meta*-ArH), 7.60 (s, 1H, 22-ArH), 7.45 (d, $^3J_{H,H}$=8.20, 2H, *meso-ortho*-ArH), 7.40 (d, $^3J_{H,H}$=8.32, *meso-ortho*-ArH), 7.16–7.31 (m, 3H, 2,3,4-ArH), 7.09 (s, 1H, 23-PyrrH), 6.42 (d, $^3J_{H,H}$=4.44,

Table 2. Crystallographic Data for **1**, **2**, and **3**.

compound	**1**	**2**	**3**
empirical formula	$C_{38}H_{33}N_3$	$C_{38}H_{33}N_3O$	$C_{38}H_{33}N_3O$
molar mass [g mol^{-1}]	531.67	547.67	547.67
crystal syst	Monoclinic	Monoclinic	Monoclinic
space group	$P2_1/n$	$P2_1/n$	$P2_1/n$
a [Å]	11.8682(4)	16.531(2)	17.069(3)
b [Å]	14.8331(4)	10.0937(16)	10.047(2)
c [Å]	16.0432(5)	18.392(3)	18.578(4)
β [°]	101.750(2)	111.677(4)	115.17(3)
V [Å^3], Z	2765.10(15), 4	2851.8(7), 4	2883.7(10), 4
D [Mg m^{-3}]	1.277	1.276	1.261
T [K]	100.0(1)	100(2)	100.0(1)
F(000)	1128	1160	1160
absorption coefficient [mm^{-1}]	0.075	0.077	0.076
θ range [°]	1.89 to 26.51	1.42 to 25.07	1.36 to 25.02
reflections collected	5711	19604	19184
independent reflections	5711	5038	5070
data/restraints/param	5711/0/371	5038/0/383	5070/0/380
R_1[a]	0.0428	0.0563	0.0371
wR_2[b]	0.0867	0.0724	0.0510
GOF on F^2	0.913	1.025	0.668
largest diff. peak and hole [e Å^{-3}]	0.245, −0.221	0.265, −0.259	0.185, −0.167

[a] $R_1 = \Sigma|F_0| - |F_c|/\Sigma|F_0|$. [b] $wR_2 = [\Sigma[\omega(F_0^2 - F_c^2)^2]/\Sigma[\omega(F_0^2)^2]]^{1/2}$.

1H, 14-PyrrH), 6.37 (d, $^3J_{H,H}$ = 3.96, 1H, 19-PyrrH), 6.25 (d, $^3J_{H,H}$ = 3.84, 18-PyrrH), 5.87 (d, $^3J_{H,H}$ = 4.44, 1H, 13-PyrrH), 3.929 (s, 3H, OCH_3), 3.932 (s, 3H, OCH_3), 1.81 (s, 6H, CH_3), 1.77 ppm (s, 6H, CH_3); HRMS (ES): *m*/*z* (%) calcd for $C_{42}H_{38}N_3O_5$: 664.2811 $[M+H]^+$; found: 664.2759 (100).

6: R_f = 0.20 (hexane/CH_2Cl_2/ethylacetate = 7:3:2); UV/Vis (CH_2Cl_2): $\lambda(\varepsilon)$ = 570 (17800), 398 (16600), 312 nm (21400); ^{1}H NMR (400 MHz, $CDCl_3$, 25 °C): δ = 12.05 (br, 1H, NH), 9.30 (s, 1H, NH), 8.01–8.05 (ab quartet, 4H, *meso-meta*-ArH), 7.78 (s, 1H, 22-ArH), 7.43 (d, $^3J_{H,H}$ = 8.24, 2H, *meso-ortho*-ArH), 7.33 (d, $^3J_{H,H}$ = 8.24, *meso-ortho*-ArH), 7.18–7.30 (m, 3H, 2,3,4-ArH), 6.57 (d, $^3J_{H,H}$ = 4.36, 1H, 19-PyrrH), 6.44 (d, $^3J_{H,H}$ = 4.36, 1H, 18-PyrrH), 6.19 (d, $^3J_{H,H}$ = 4.36, 1H, 14-PyrrH), 5.81 (d, $^3J_{H,H}$ 4.32, 1H, 13-PyrrH), 5.68 (d, $^4J_{H,H}$ = 1.80, 1H; 23-PyrrH), 3.93 (s, 3H, OCH_3), 3.89 (s, 3H, OCH_3), 1.84 (s, 6H, CH_3), 1.48 ppm (s, 6H, CH_3); HRMS (ES): *m*/*z* (%) calcd for $C_{42}H_{38}N_3O_5$: 664.2811 $[M+H]^+$; found: 664.2802 (100).

X-ray Structure Determination

Crystal data and other details of the structure analysis are presented in Table 2. Suitable crystals of **1**, **2**, and **3** were obtained by slow diffusion of *n*-hexane into a CH_2Cl_2 solution at room temperature. Crystals were mounted on the end of a glass fiber. The diffraction frames were integrated using the SAINT package[32] and corrected for absorption with SADABS.[33] The structure was solved by direct methods, expanded using Fourier techniques, and refined on F^2 by full-matrix least-squares methods. All refinements were carried out using the program SHELXL-97.[34] All non-hydrogen atoms were assigned anisotropic displacement parameters and refined without positional constraint. The positions of hydrogen on the pyrrolic nitrogens for **2** and **3** can be clearly confirmed from the density map but further refinements gave elongated N–H bonds and were constrained to idealized distances. All other hydrogen atoms were introduced at idealized positions (C–H = 0.96) and were allowed to ride on the parent carbon atom. The drawing of the crystal structures with atom numbering at the 50% probability level of displacement ellipsoids are shown in Figure S11 to S13 of the Supporting Information.

CCDC 700796, 700797, and 700798 contain the supplementary crystallographic data for this paper. These data can be obtained free of charge from The Cambridge Crystallographic Data Centre at www.ccdc.cam.ac.uk/data_request/cif.

DFT Calculation

DFT calculations were performed with the Gaussian 03 program.[29] Geometry optimizations were carried out within unconstrained C1 symmetry. Starting geometries were obtained from the crystal structures. Becke's three parameters exchange functional[35] with the gradient corrected correlation formula of Lee, Yang, and Parr [DFT-B3LYP][36] was used with the 6-31g** basis set to optimize the geometry. Single-point calculations were carried out at B3LYP/6-311g** level of theory. Harmonic vibrational frequencies were calculated using analytical second derivatives for all structures. Calculated vibrational frequencies show that the obtained geometries represent true minima since no imaginary frequencies were found. In all calculation, convergence was reached when the relative change in the density matrix between subsequent iteration was less than 1×10^{-8}.

Acknowledgements

The financial support from National Science Council of Taiwan and Academia Sinica is greatly acknowledged. We also thank National Center for High Performance Computing and Computing Center of Academia Sinica for the assistance with the theoretical calculations.

[1] M. Stępień, L. Latos-Grażyński, *Acc. Chem. Res.* **2005**, *38*, 88.
[2] J. L. Sessler, D. Seidel, *Angew. Chem.* **2003**, *115*, 5292; *Angew. Chem. Int. Ed.* **2003**, *42*, 5134.
[3] J. L. Sessler, W.-S. Cho, V. Lynch, V. Král, *Chem. Eur. J.* **2002**, *8*, 1134.
[4] P. J. Chmielewski, L. Latos-Grażyński, K. Rachlewicz, T. Głowiak, *Angew. Chem.* **1994**, *106*, 805; *Angew. Chem. Int. Ed. Engl.* **1994**, *33*, 779.
[5] H. Furuta, T. Asano, T. Ogawa, *J. Am. Chem. Soc.* **1994**, *116*, 767.
[6] K. Berlin, E. Breitmaier, *Angew. Chem.* **1994**, *106*, 1356; *Angew. Chem. Int. Ed. Engl.* **1994**, *33*, 1246.
[7] T. Lash, *Angew. Chem.* **1995**, *107*, 2703; *Angew. Chem. Int. Ed. Engl.* **1995**, *34*, 2533.
[8] H. Furuta, H. Nanami, T. Morimoto, T. Ogawa, V. Kral, J. S. Sessler, V. Lynch, *Chem. Asian J.* **2008**, *3*, 592.
[9] L. Latos-Grażyński in *The Porphyrin Handbook*, *Vol. 2* (Eds.: K. M. Kadish, K. M. Smith, R. Guilard), Academic Press, New York, **2000**, pp. 361–416.
[10] T. Lash in *The Porphyrin Handbook*, *Vol. 2* (Eds.: K. M. Kadish, K. M. Smith, R. Guilard), Academic Press, New York, **2000**, pp. 125–200.
[11] a) G. van Koten, *Pure Appl. Chem.* **1989**, *61*, 1681; b) M. H. P. Rietveld, D. M. Grove, G. van Koten, *New J. Chem.* **1997**, *21*, 751; c) R. A. Gossage, L. A. van de Kuil, G. van Koten, *Acc. Chem. Res.* **1998**, *31*, 423.
[12] a) M. Gozin, A. Weisman, Y. Ben-David, D. Milstein, *Nature* **1993**, *364*, 699; b) N. Ashkenazi, A. Vigalok, S. Parthiban, Y. Ben-David, L. J. W. Shimon, J. M. L. Martin, D. Milstein, *J. Am. Chem. Soc.* **2000**, *122*, 8797.
[13] G. R. Newkome, W. E. Puckett, V. K. Gupta, G. E. Kiefer, *Chem. Rev.* **1986**, *86*, 451.
[14] G. R. Giesbrecht, G. S. Hanan, J. E. Kickham, S. J. Loeb, *Inorg. Chem.* **1992**, *31*, 3286.

[15] T. D. Lash, S. T. Chaney, *Angew. Chem.* **1997**, *109*, 867; *Angew. Chem. Int. Ed. Engl.* **1997**, *36*, 839.
[16] M. Stępień, L. Latos-Grażyński, *Chem. Eur. J.* **2001**, *7*, 5113.
[17] M. Stępień, L. Latos-Grażyński, *J. Am. Chem. Soc.* **2002**, *124*, 3838.
[18] M. Stępień, L. Latos-Grażyński, T. D. Lash, L. Szterenberg, *Inorg. Chem.* **2001**, *40*, 6892.
[19] M. Stępień, L. Latos-Grażyński, *Org. Lett.* **2003**, *5*, 3379.
[20] M. Stępień, L. Latos-Grażyński, L. Szterenberg, J. Panek, Z. Latajka, *J. Am. Chem. Soc.* **2004**, *126*, 4566.
[21] C.-H. Hung, F.-C. Chang, C.-Y. Lin, K. Rachlewicz, M. Stępień, L. Latos-Grażyński, G.-H. Lee, S.-M. Peng, *Inorg. Chem.* **2004**, *43*, 4118.
[22] C.-H. Hung, G.-F. Chang, A. Kumar, G.-F. Lin, L.-Y. Luo, W.- M. Ching, E. W.-G. Dia, *Chem. Commun.* **2008**, 978.
[23] a) H. Furuta, T. Ishizuka, A. Osuka, Y. Uwatoko, Y. Ishikawa, *Angew. Chem.* **2001**, *113*, 2385; *Angew. Chem. Int. Ed.* **2001**, *40*, 2323; b) I. Schmidt, P. J. Chmielewski, *Tetrahedron Lett.* **2001**, *42*, 6389.
[24] M. Pawlicki, L. Latos-Grażyński, *Chem. Rec.* **2006**, *6*, 64.
[25] A. S. F. Boyd, M. J. Frost, N. M. Howarth, *J. Mol. Struct.* **2004**, *688*, 149.
[26] M. Adler, B. Laughlin, S. G. Lieb, *Phys. Chem. Chem. Phys.* **1999**, *1*, 5333.
[27] N. A. Prokopenko, I. A. Bethea, C. J. Clemens IV, A. Klimek, K. Wargo, C. Spivey, K. Waziri, A. Grushow, *Phys. Chem. Chem. Phys.* **2002**, *4*, 490.
[28] A. Ghosh in *The Porphyrin Handbook*, *Vol. 7* (Eds.: K. M. Kadish, K. M. Smith, R. Guilard), Academic Press, New York, **2000**, pp. 1–31.
[29] Gaussian 03 (Revision D.02), M. J. Frisch, G. W. Trucks, H. B. Schlegel, G. E. Scuseria, M. A. Robb, J. R. Cheeseman, J. A. Montgomery, Jr., T. Vreven, K. N. Kudin, J. C. Burant, J. M. Millam, S. S. Iyengar, J. Tomasi, V. Barone, B. Mennucci, M. Cossi, G. Scalmani, N. Rega, G. A. Petersson, H. Nakatsuji, M. Hada, M. Ehara, K. Toyota, R. Fukuda, J. Hasegawa, M. Ishida, T. Nakajima, Y. Honda, O. Kitao, H. Nakai, M. Klene, X. Li, J. E. Knox, H. P. Hratchian, J. B. Cross, V. Bakken, C. Adamo, J. Jaramillo, R. Gomperts, R. E. Stratmann, O. Yazyev, A. J. Austin, R. Cammi, C. Pomelli, J. W. Ochterski, P. Y. Ayala, K. Morokuma, G. A. Voth, P. Salvador, J. J. Dannenberg, V. G. Zakrzewski, S. Dapprich, A. D. Daniels, M. C. Strain, O. Farkas, D. K. Malick, A. D. Rabuck, K. Raghavachari, J. B. Foresman, J. V. Ortiz, Q. Cui, A. G. Baboul, S. Clifford, J. Cioslowski, B. B. Stefanov, G. Liu, A. Liashenko, P. Piskorz, I. Komaromi, R. L. Martin, D. J. Fox, T. Keith, M. A. Al-Laham, C. Y. Peng, A. Nanayakkara, M. Challacombe, P. M. W. Gill, B. Johnson, W. Chen, M. W. Wong, C. Gonzalez, J. A. Pople, Gaussian, Inc., Wallingford, CT, **2004**.
[30] A. Ghosh, T. Wondimagegn, H. Nilsen, *J. Phys. Chem. B* **1998**, *102*, 10459.
[31] Z. Meng, W. R. Carper, *J. Mol. Struct.* **2002**, *588*, 45.
[32] SAINT, v. 5.0, Bruker Analytical X-Ray Systems, Madison, WI.
[33] G. M. Sheldrick, *SADABS*, Empirical Absorption Correction Program, University of Göttingen, Göttingen (Germany), **1996**.
[34] G. M. Sheldrick, *SHELXL-97*, A Program for the Refinement of Crystal Structures, University of Göttingen, Göttingen (Germany), **1997**.
[35] a) A. D. Becke, *Phys. Rev. A* **1988**, *38*, 3098; b) A. D. Becke, *J. Chem. Phys.* **1993**, *98*, 1372; c) A. D. Becke, *J. Chem. Phys.* **1993**, *98*, 5648.
[36] C. Lee, W. Yang, R. G. Parr, *Phys. Rev. B* **1988**, *37*, 785.

Received: July 23, 2008
Revised: August 27, 2008
Published online: November 4, 2008

